PCCP

PAPER

View Article Online
View Journal | View Issue

Cite this: *Phys. Chem. Chem. Phys.*, 2019, **21**, 13462

Chemically-resolved determination of hydrogenated graphene–substrate interaction†

Anders L. Jørgensen,‡[a] David A. Duncan,[b] Claus F. P. Kastorp,[a] Line Kyhl,[a] Zeyuan Tang,[a] Albert Bruix,[c] Mie Andersen,[c] Bjørk Hammer,[a] Tien-Lin Lee,[b] Liv Hornekær[a] and Richard Balog*[a]

Received 11th April 2019,
Accepted 3rd June 2019

DOI: 10.1039/c9cp02059d

rsc.li/pccp

Functionalization of graphene on Ir(111) is a promising route to modify graphene by chemical means in a controlled fashion at the nanoscale. Yet, the nature of such functionalized sp^3 nanodots remains unknown. Density functional theory (DFT) calculations alone cannot differentiate between two plausible structures, namely true graphane and substrate stabilized graphane-like nanodots. These two structures, however, interact dramatically differently with the underlying substrate. Discriminating which type of nanodots forms on the surface is thus of paramount importance for the applications of such prepared nanostructures. By comparing X-ray standing wave measurements against theoretical model structures obtained by DFT calculations we are able to exclude the formation of true graphane nanodots and clearly show the formation graphane-like nanodots.

Introduction

Chemical functionalization of graphene by hydrogen has been shown to induce novel properties in graphene sheets. For randomly chemisorbed hydrogen, effects such as increased spin–orbit coupling[1] and ferromagnetism[2,3] have been observed. A nanometer scale periodic functionalization on the other hand has been shown to open a bandgap in graphene where the size of the gap can be controlled by the periodicity of the hydrogen pattern.[4] A periodic hydrogen pattern can be prepared in graphene on Ir(111) due to a site selective reactivity driven by the moiré superstructure. Two regions of the moiré unit cell, namely the FCC and the HCP regions, are efficiently hydrogenated.[5,6] However, at high temperature ($\approx$600 K) only the HCP regions are populated forming a triangular periodic pattern of H-clusters on macroscopically large areas.[7] Here, using the X-ray standing wave (XSW) technique we aim to reveal the geometrical structure of graphene hydrogenated at the HCP regions within the moiré. The primary question, to be addressed by these measurements, is whether the hydrogenation of the graphene in these locations results in a true graphane nanodot configuration, where every C atoms is bound to one hydrogen atom attached alternately from above and below,[8] or whether the carbon atoms form a graphane-like configuration with alternating carbon atoms forming a bond with a hydrogen atom and a surface Ir atom.[4] This difference between the two structures has important implications. While the graphane-like cluster interacts strongly with the substrate due to C–Ir bond formation, the graphane cluster weakens the interaction owing to the presence of C–H bonds in the gap between graphene and Ir.

Previous STM measurements[4] demonstrated lateral ordering of H-nanodots and a preference for formation in the HCP regions. However, the significant alteration to the electronic structure of hydrogenated graphene precludes drawing any certain conclusion about the vertical geometric structure of the hydrogenated regions and especially what is occurring below them. DFT calculations predict that both structures are stable with very similar formation energies[9] and thus cannot differentiate between them. Hence a spectroscopic probe of the structure is required.

XSW is a highly sensitive method capable of measuring adsorbate-substrate distances with sub-ångstrom resolution.[6,10] An XSW field is created by interference between the incoming and the bulk diffracted X-ray waves under Bragg diffraction condition. The standing wave field extending above the surface exhibits the periodicity of the Bragg plane spacing, d. To generate XSW with the (111) reflection of iridium (d = 2.2164 Å), the photon energy is tuned to around 2797 eV. An adsorbate experiencing the

[a] *Department of Physics and Astronomy and Interdisciplinary Nanoscience Center (iNANO), Aarhus University, 8000 Aarhus C, Denmark. E-mail: balog@phys.au.dk*
[b] *Diamond Light Source Ltd, Harwell Science and Innovation Campus, Didcot, OX11 0DE, UK*
[c] *Chair for Theoretical Chemistry and Catalysis Research Center, Technische Universität München, Lichtenbergstr. 4, D-85747 Garching, Germany*

† Electronic supplementary information (ESI) available: Includes complete analysis of adsorption heights for all DFT calculated model structures. See DOI: 10.1039/c9cp02059d

‡ Present address: Newtec Engineering A/S – Stærmosegårdsvej 18, 5000 Odense M, Denmark and University of Southern Denmark, MCI – Alsion 2, 6400 Sønderborg, Denmark.

XSW field emits electrons with a yield proportional to the standing wave intensity at its position. By measuring the variation of the photoelectron intensity during a photon energy scan around the Bragg energy, which accordingly shifts the phase of the standing wave, we obtain a position specific yield profile for the adsorbate. Utilizing dynamical diffraction theory,[10,11] the intensity profile is fitted with two structural parameters referred to as the coherent position P^H and the coherent fraction F^H. These are related to the relative mean height of the adsorbate and a spread in height around the mean value, respectively.[12]

Results and discussion

Graphene on Ir(111) was synthesized by combined temperature programmed desorption (TPD) and chemical vapor deposition (CVD)[13] (see methods for details). At first, the quality of the graphene layer was inspected. Using X-ray photoelectron spectroscopy (XPS) measurements at photon energy of 435 eV, we obtain a single sp^2 component in the C1s spectrum as expected. XSW measurements on the clean graphene (not shown) yield structural parameters $P^{111} = 0.54 \pm 0.01$ and $F^{111} = 0.74 \pm 0.01$ that are in line with the earlier results obtained by Busse *et al.*[6] As the coherent positions are given as relative heights modulo and normalized to $d^{111} = 2.2164$ Å, the corresponding mean height is $\bar{h} = (n + P^{111}) \times d^{111}$, where n is an integer. Here only $n = 1$ yields a reasonable height, which is $\bar{h} = 3.41 \pm 0.04$ Å. This value is in good agreement with the vdW-corrected density functional theory (DFT) calculations, $\bar{h} = 3.54$ Å, when referenced against a projected bulk-like truncation (see ESI† for explanation). Additionally the dependence of coherent fraction and the coherent position on the graphene coverage has been studied previously.[14] These studies revealed that the coherent position of sp^2 carbon remains unaltered with increasing coverage, but the coherent fraction decreases due to an increasing stress in large graphene areas. When using these results, the F^{111} value in our study gives coverage of about 0.63 ML, which is lower than the expected 1 ML. The lower coverage estimated from the coherent fraction value may, however, be due to the different growth procedures used in the two studies that consequently lead to different extent of stress in graphene sheet (see methods for graphene growth). We note, however, that for sufficiently large graphene islands the coverage plays negligible role for the hydrogenation studies discussed in the article.

A periodic hydrogen pattern was prepared by exposing the graphene covered Ir(111) to hot H atoms at a sample temperature of 600 K. Fig. 1a shows the corresponding C1s spectrum fitted with two components using a Doniach Sunjic function and a Shirley type background. The two distinguishable components are assigned to sp^2 (grey) and sp^3 (brown) carbon, representing clean and hydrogenated graphene regions, respectively.[15] After the initial XPS measurements we excited the Ir(111) Bragg reflection to measure the XSW-modulated intensity profiles of the individual C1s components. Fig. 1b shows the XSW-modulated C1s intensities of the sp^2 and sp^3

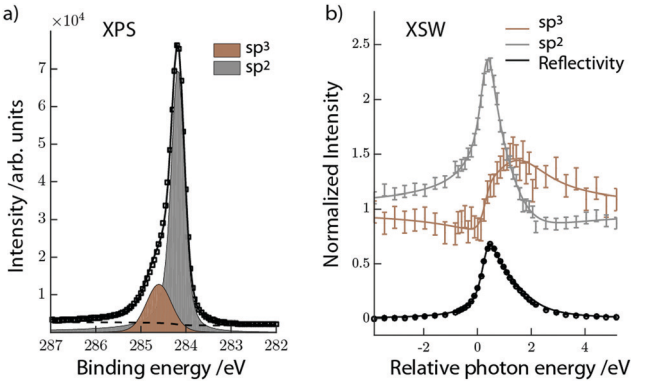

Fig. 1 (a) XPS spectrum of C1s of periodically hydrogenated graphene. The sp^2 and sp^3 components represent clean and hydrogenated areas, respectively. (b) XSW photoemission profiles of the sp^2 and sp^3 intensities across the interval of energies satisfying the Bragg diffraction. Dots and lines in the figure represent experimental data and fits to the data, respectively.

components in graphene functionalized at high temperature together with their best fits. The coherent position obtained for the sp^2 C is $P^{111} = 0.56 \pm 0.01$, which is clearly very similar to the value found for bare graphene. The adsorption height is then $\bar{h} = 3.46 \pm 0.02$ Å, corresponding to $n = 1$. For the sp^3 component we measure coherent position $P^{111} = 0.02 \pm 0.03$, which corresponds to two feasible adsorption heights, $\bar{h} = 2.26 \pm 0.07$ Å and $\bar{h} = 4.48 \pm 0.07$ Å, with $n = 1$ and 2, respectively. Neither of these two heights can be immediately ruled out because two types of H-clusters are being considered here, as depicted in Fig. 2. The graphene-like structure where approximately half of the sp^3 C atoms within the cluster interact strongly with the underlying Ir, and are thus positioned closer to the substrate than the clean graphane parts (Fig. 2b) and the real graphane cluster where all of the sp^3 C atoms are covalently bound to H atoms, and are thus pushed further away from the substrate than the clean graphene parts (Fig. 2c). To determine which cluster is present on the surface, DFT calculations using optimized moiré supercells and vdW-corrected density functionals were employed. The calculated model structures consist of a 10×10 supercell of graphene on a 9×9 supercell of iridium with a hydrogen cluster positioned on the HCP region of the graphene/Ir(111) moiré. A wide range of H-clusters were explored, specifically, 13–52H atoms for the graphane cluster and 3–27H atoms for the graphane-like cluster. The theoretical coherent positions and fractions (see ESI,† for more details) and adsorption heights of sp^2 and sp^3 carbon atoms for all model structures, compared against the experimental values, are summarised in Table 1 and shown in Fig. 3. Comparing the calculated values for the graphane structure model (Fig. 3, green symbols) with the experimentally determined heights (black line) show no agreement at any H-cluster size allowing us to exclude the formation of graphane clusters in this system. The graphane-like structure model (Fig. 3, red symbols), however, agrees remarkably well with the experimental values with specifically strong agreement for the 19H cluster. The corresponding structure of the 19H cluster is depicted in Fig. 2a and b.

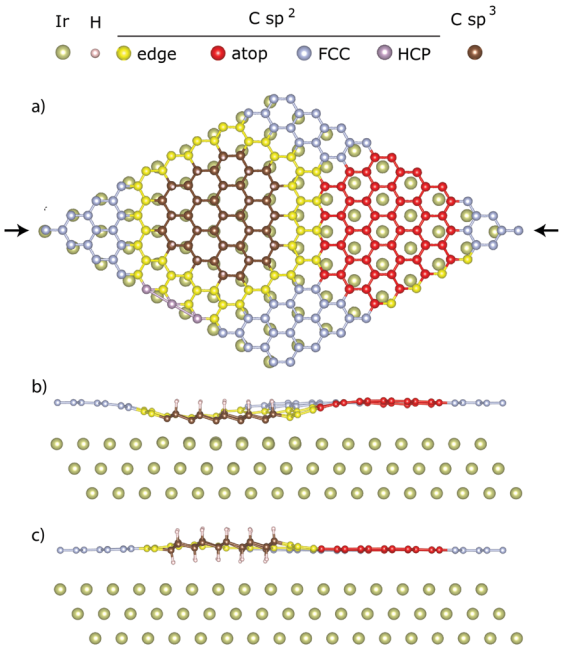

Fig. 2 DFT-optimized structures of graphene on Ir patterned with hydrogen in the HCP region of the graphene–Ir moiré, consisting of 10 × 10 unit cells of graphene on 9 × 9 unit cells of iridium. The sp^3 hybridized carbon atoms in the HCP region are marked brown. The sp^2 hybridized carbon atoms are divided into four sub-categories: on atop region (red), on HCP region (purple), on FCC region (silver) and at the H-cluster edge (yellow). (a) A top view of the 19H (37H) H-cluster (for clarity only one Ir layer is shown). (b) and (c) Cross-sectional view of the 19H graphane-like and the 37H graphane cluster structure, respectively. The arrows in (a) indicate the cross-sectional plane.

Table 1 Comparison of coherent position (P^{111}), mean adsorption height ($\bar{h}$) and coherent fraction (F^{111}) derived from the XSW measurements and from the DFT optimized graphane-like and graphane clusters of various sizes

	P^{111}		$\bar{h}$/Å		F^{111}	
#H	sp^2	sp^3	sp^2	sp^3	sp^2	sp^3
DFT-graphane						
13H	0.60	0.69	3.54	3.75	0.97	0.75
22H	0.61	0.77	3.57	3.92	0.97	0.75
37H	0.62	0.78	3.59	3.95	0.96	0.72
52H	0.63	0.84	3.61	4.07	0.93	0.72
XSW						
	0.56(1)	0.02(3)	3.46(2)	4.47(7) or 2.26(7)	0.41(2)	0.43(5)
DFT-graphane-like						
3H	0.57	0.12	3.48	2.48	0.77	0.87
7H	0.57	0.11	3.48	2.46	0.66	0.78
12H	0.56	0.1	3.46	2.44	0.59	0.77
19H	0.55	0.08	3.44	2.39	0.55	0.77
27H	0.54	0.08	3.41	2.39	0.50	0.76

Our recent work suggests that 5–10% H-coverage per moiré results in the most stable graphane-like structures.[7] This coverage corresponds to 10–20H graphane-like clusters in the present study. The 19H cluster found here is thus in excellent agreement with the earlier estimation of the most stable cluster

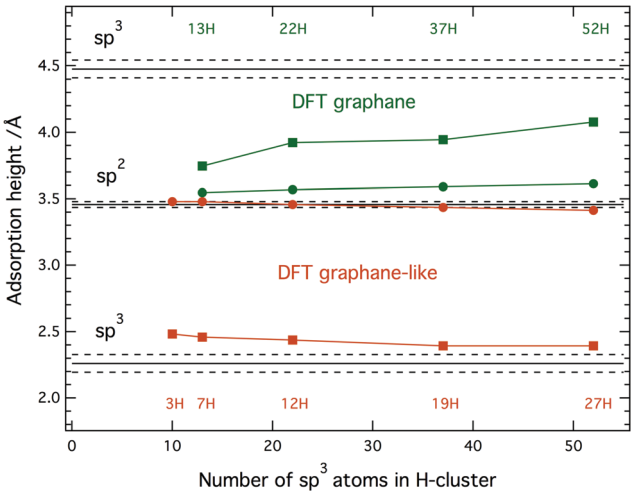

Fig. 3 Adsorption heights of sp^2 and sp^3 C1s components obtained from the present XSW analysis for hydrogenated graphene (black, dashed lines represent error bars) and from DFT-optimized graphane-like (red) and graphane (green) structures. Square and round symbols in the theoretical data represent sp^3 and sp^2 components, respectively.

size. All sp^2 carbon atoms in Fig. 2 are further divided into four sub-categories depending on the position within the moiré they occupy. Detailed analysis of these sub-groups in the graphane-like model structure (see Table S1 in ESI†) then reveals that the adsorption height of the FCC region, marked silver in Fig. 2, is higher than the same region in bare graphene on iridium, gradually shifting from 3.52 Å to 3.59 Å with increasing cluster size. At the same time the adsorption height of sp^2 atoms in the atop region (marked red) decreases from 3.68 Å to 3.61 Å. Thus the heights of the FCC and atop regions have approached each other and on average they have remained at the same mean height as in bare graphene on iridium (≈3.59 Å). Despite this flattening of the FCC and atop region a decrease in the total coherent position of the sp^2 atoms, as the H-cluster size increases, is predicted by the DFT calculations, as seen in Fig. 3. This is caused by sp^2 atoms at the edge of graphane-like cluster (marked yellow in Fig. 2), which are dragged closer to the substrate due to pinning effect. For the 27H model edge atoms comprise ∼1/3rd of the residual sp^2 atoms within the moiré. In fact, due to the adjustment of carbon atom heights in the FCC and ATOP regions in the presence of the graphane-like clusters the shape of hydrogenated graphene approaches the egg box model[16] also found for graphene pinned by a periodic array of platinum clusters.[17]

Though the graphane-like model structure agrees much better with the experiment, we have yet to address the persistent higher position of sp^3 atoms appearing in the calculations even for large H-clusters (Table 1 and Fig. 3). We attribute this apparent discrepancy to the fact that in modelled graphane-like cluster structures (12H and 19H), the number of sp^3 carbon atoms bonded to hydrogen is slightly higher than those bonded to iridium. Noting, that the selective adsorption height of sp^3 carbon atoms involved in C–H bonds and in C–Ir bonds is 2.62 Å and 2.15 Å and thus above and below the experimental

value, respectively. In the experiment the ratio between carbon atoms involved in C–H and C–Ir bonds will be lowered due to the variety of clusters structures formed[4] but also due to the presence of H-vacancies in the clusters. These vacancies are generally introduced *via* Eley–Rideal hydrogen abstraction reaction that competes with hydrogen addition reaction during the hydrogenation experiments.[18] These effects are clearly not captured in structural parameters obtain from the theoretical model structures were for given value only a single type of H-cluster is considered. Nevertheless, the above-mentioned effects have a tendency to lower the total adsorption height of sp^3 atoms. Finally we also comment on the experimental coherent fractions that always appear lower in value than the theoretical ones (see Table 1 for comparison). In general a lower coherent fraction in experiment, compared to DFT, is to be expected due to the latter being estimated for a system at 0 K. The DFT value therefore does not adopt distortions induced by thermal vibrations. Also, a natural variation in the size of the clusters as mentioned above will further decrease the experimental coherent fraction.

Conclusions

In conclusion, we have determined the structure and interaction of graphene on Ir(111) upon patterned hydrogenation at high temperature using the XSW technique and DFT. The hydrogenated graphene regions comprise nanoclusters in the HCP region of graphene/Ir moiré that are found at a mean height of 2.26 ± 0.07 Å. The mean height of sp^2 carbon atoms remains broadly unaffected at 3.46 ± 0.02 Å, though theoretical calculations indicate a reduced corrugation between atop and FCC areas. Additionally, the size of H-clusters, estimated from the corrugation of graphene in the present study, agrees remarkably well with the size of most stable graphane-like clusters as found by DFT calculations. We thus decisively conclude that the H-clusters induce strong coupling of graphene to the underlying substrate and thus determine the reaction pathway that has to be considered when altering the properties of graphene sheets on metal substrates by chemical functionalization.

Experimental

Materials and methods

Sample preparation. The Ir(111) crystal was cleaned by cycles of Ar^+ sputtering at room temperature (RT) followed by vacuum annealing to 1400 K. Prior to graphene growth the sample is cycled three times between 500 K and 1100 K in an oxygen atmosphere ($p = 4 \times 10^{-7}$ mbar) in order to remove any residual carbon on the surface. Single layer graphene was grown in two steps. First we deposited ethylene ($p = 2 \times 10^{-7}$ mbar) on the Ir sample for 100 s while keeping the sample at RT. Then the sample was flashed to 1470 K. Hereafter the sample temperature was reduced to 1200 K while at the same time the ethylene pressure was increased to 4×10^{-6} mbar. The sample was then kept at this condition for three minutes. Finally, the ethylene inlet was closed, and the sample was flashed again to 1400 K before cooling down to RT.

The atomic hydrogen beam was formed by passing molecular hydrogen through a hot (2000 K) tungsten capillary. Exposure to atomic hydrogen was conducted at a hydrogen background pressure of $p_{bcg} = 4 \times 10^{-7}$ mbar while keeping the sample at 600 K in front of the beam for about 2 × 20 min. This results in a saturated hydrogen coverage for the given deposition condition. After the hydrogenation process the sample is cooled down to RT.

Experimental method. Our data were obtained at I09 beamline at Diamond Light Source, UK. The I09 beam line provides access to both the 'hard' and 'soft' X-ray regimes by utilising two separate undulators as the X-ray sources, one monochromated by a double silicon (111) single crystal monochromator ('hard' X-ray) and the other by a plane grating monochromator (400 lines per mm, 'soft' X-ray). The permanent endstation, mounted behind the final port of the beam line, has the standard facilities for *in situ* sputtering and annealing of single crystal samples. The X-ray photoelectron spectra and the photoemission profiles were both acquired utilizing a VG Scienta EW4000 HAXPES hemispherical electron analyser (angular acceptance of ±30°), which was mounted perpendicular to the direction of the incident light, in the plane of the photon polarization (linear horizontal). The XSW measurements were acquired in a back reflection geometry (Bragg angle of almost 90°), and the intensity of the reflected light was measured with a CCD-camera from a fluorescent screen that was mounted in the port through which the incident light passed. The non-dipolar effects were modelled using a backward–forward asymmetry parameter, Q, which was calculated theoretically using the average angle acquired on the analyser (=18°).[19] The data presented in Fig. 1b represent the average over 9 repeated measurements, each of which was acquired from a different spot on the sample. The XSW acquisition time at each single spot was 19 minutes. To avoid any beam-induced damage of the sample, the beam was detuned by a factor of 5 by altering the undulator gap. C1s XP spectra, utilising the hard X-ray light, were acquired before and after the XSW measurements to monitor potential beam damage, however no such damage was observed. All XPS and XSW measurements were performed while keeping the sample at RT.

Computational details. The density functional theory (DFT) calculations were performed using the real-space, grid-based projector augmented wave method GPAW code[20,21] together with the Atomic Simulation Environment (ASE).[22] Exchange and correlation effects were accounted for using the optB88-vdW functional,[23] which also satisfactorily accounts for vdW interactions.[24,25] The Ir/graphene interface was described using a supercell model consisting of a (10 × 10) graphene sheet on a three-layered (9 × 9) Ir(111) surface, which is very close to the experimentally observed incommensurate moiré unit mesh of (10.32 × 10.32) graphene lattice vectors to (9.32 × 9.32) Ir lattice vectors.[26] In order to obtain a commensurate structure in the used supercell model, either the metal or the graphene lattice

constant must be modified. Since we are mainly interested in the properties of the graphene sheet (*i.e.* it's hydrogenation), we chose to fix the lateral size of the supercell to ten times the optimized graphene lattice constant of 2.465 Å. This resulted in a slight strain of the average Ir lattice constant of −1.12% parallel to the slab with respect to its optimized value of 3.92 Å. Structure relaxations were performed using Broyden–Fletcher–Goldfarb–Shanno (BFGS) algorithm as implemented in ASE. During the relaxation the bottom metal layer was kept fixed and the remaining atoms were relaxed until the maximum force on each atom fell below 0.02 eV $Å^{-1}$. This means that the Ir atoms are free to adjust their spacing perpendicular to the slab to compensate for the strain parallel to the slab, and we do therefore not expect the small strain to influence the adsorption properties of the graphene sheet. Two-dimensional periodic boundary conditions were employed parallel to the slab. In the direction perpendicular to the slab a vacuum region of 6 Å was included on both sides of the slab, *i.e.* a total of 12 Å vacuum was used. Only the Γ point was used to sample the Brillouin zone. The grid spacing was 0.1768 Å.

Conflicts of interest

There are no conflicts to declare.

Acknowledgements

We acknowledge financial support from VILLUM FONDEN (research grant no. 17547 and 16562 and grant no. 11744 – Villum Centre of Excellence for Dirac. Materials), the Danish Council for Independent Research (grant no. 5137-00049B), Innovation Fund Denmark (NIAGRA) (grant no. 5184-00018B), the European Research Council (CoG GRANN, grant no. 648551), the European Union (EU) and Horizon 2020 funding award under the Marie Skłodowska-Curie action to the EUROPAH consortium, grant number 722346. Affiliation with the Center for Integrated Materials Research (iMAT) at Aarhus University is gratefully acknowledged. We also acknowledge Diamond Light Source for time on beamline I09 under proposal SI16243-1 and thank the I09 technical staff for assistance and support during the measurements.

Notes and references

1 A. Avsar, J. H. Lee, G. K. W. Koon and B. Özyilmaz, *2D Mater.*, 2015, **2**, 044009.
2 W. K. Lee, K. E. Whitener, J. T. Robinson and P. E. Sheehan, *Adv. Mater.*, 2015, **27**(10), 1774–1778.
3 M. V. Ulybyshev and M. I. Katsnelson, *Phys. Rev. Lett.*, 2015, **114**, 1–5.
4 R. Balog, B. Jørgensen, L. Nilsson, M. Andersen, E. Rienks, M. Bianchi, M. Fanetti, E. Lægsgaard, A. Baraldi and S. Lizzit, *et al.*, *Nat. Mater.*, 2010, **9**, 315–319.
5 A. T. N'Diaye, J. Coraux, T. N. Plasa, C. Busse and T. Michely, *New J. Phys.*, 2008, **10**, 043033.
6 C. Busse, P. Lazic, R. Djemour, J. Coraux, T. Gerber, N. Atodiresei, V. Caciuc, R. Brako, A. T. N'Diaye and S. Blügel, *et al.*, *Phys. Rev. Lett.*, 2011, **107**, 1–4.
7 J. H. Jørgensen, A. G. Čabo, R. Balog, L. Kyhl, M. N. Groves, A. M. Cassidy, A. Bruix, M. Bianchi, M. Dendzik and M. A. Arman, *et al.*, *ACS Nano*, 2016, **10**, 10798–10807.
8 T. Balgar, H. Kim and E. Hasselbrink, *J. Phys. Chem. Lett.*, 2013, **4**, 2094–2098.
9 Based on our DFT optimised structures we obtain formation energies that vary depending on the cluster size. The values are, however, similar for both types of clusters of the same size (see ESI,† Fig. S3). For the most stable clusters the formation energy is approx. 2.4–2.5 eV per H. What type of H-cluster dominates on the surface is thus most likely dictated by kinetic barriers for adsorption/desorption and intercalation/deintercalation of hydrogen.
10 D. P. Woodruff, *Rep. Prog. Phys.*, 2005, **68**, 743.
11 B. W. Batterman and H. Cole, *Rev. Mod. Phys.*, 1964, **36**, 681–717.
12 J. Zegenhagen, *Phys. Scr.*, 1991, **T39**, 328–332.
13 J. Coraux, A. T. N'Diaye, M. Engler, C. Busse, D. Wall, N. Buckanie, F. J. M. Z. Heringdorf, R. V. Gastel, B. Poelsema and T. Michely, *New J. Phys.*, 2009, **11**, 023006.
14 S. Runte, P. Lazić, C. Vo-Van, J. Coraux, J. Zegenhagen and C. Busse, *Phys. Rev. B: Condens. Matter Mater. Phys.*, 2014, **89**(15), 155427.
15 R. Balog, M. Andersen, B. Jørgensen, Z. Sljivancanin, B. Hammer, A. Baraldi, R. Larciprete, P. Hofmann, L. Hornekær and S. Lizzit, *ACS Nano*, 2013, **7**, 3823–3832.
16 D. Franz, S. Runte, C. Busse, S. Schumacher, T. Gerber, T. Michely, M. Mantilla, V. Kilic, J. Zegenhagen and A. Stierle, *Phys. Rev. Lett.*, 2013, **110**, 1–5.
17 J. Knudsen, P. J. Feibelman, T. Gerber, E. Grånäs, K. Schulte, P. Stratmann, J. N. Andersen and T. Michely, *Phys. Rev. B: Condens. Matter Mater. Phys.*, 2012, **85**, 1–6.
18 T. Zecho, A. Güttler, X. Sha, D. Lemoine, B. Jackson and J. Küppers, *Chem. Phys. Lett.*, 2002, **366**, 188–195.
19 C. J. Fisher, R. Ithin, R. G. Jones, G. J. Jackson, D. P. Woodruff and B. C. C. Cowie, *J. Phys.: Condens. Matter*, 1998, **10**, L623.
20 J. J. Mortensen, L. B. Hansen and K. W. Jacobsen, *Phys. Rev. B: Condens. Matter Mater. Phys.*, 2005, **71**, 035109.
21 J. Enkovaara, C. Rostgaard, J. J. Mortensen, J. Chen, M. Dułak, L. Ferrighi, J. Gavnholt, C. Glinsvad, V. Haikola and H. A. Hansen, *et al.*, *J. Phys.: Condens. Matter*, 2010, **22**, 253202.
22 A. H. Larsen, J. J. Mortensen, J. Blomqvist, I. E. Castelli, R. Christensen, M. Dułak, J. Friis, M. N. Groves, B. Hammer and C. Hargus, *et al.*, *J. Phys.: Condens. Matter*, 2017, **29**, 273002.
23 J. Klimeš, D. R. Bowler and A. Michaelides, *J. Phys.: Condens. Matter*, 2010, **22**, 022201.
24 M. Andersen, L. Hornekær and B. Hammer, *Phys. Rev. B: Condens. Matter Mater. Phys.*, 2014, **90**, 1–9.
25 F. Mittendorfer, A. Garhofer, J. Redinger, J. Klimeš, J. Harl and G. Kresse, *Phys. Rev. B: Condens. Matter Mater. Phys.*, 2011, **84**, 2–5.
26 J. Coraux, A. T. N'Diaye, C. Busse and T. Michely, *Nano Lett.*, 2008, **8**, 565–570.